Eur. Phys. J. D **15**, 355–363 (2001)

THE EUROPEAN PHYSICAL JOURNAL D

EDP Sciences

Formation of ultracold molecules via photoassociation with blue detuned laser light

M.-L. Almazor[1], O. Dulieu[1,a], F. Masnou-Seeuws[1], R. Beuc[2], and G. Pichler[1,2]

[1] Laboratoire Aimé Cotton, CNRS, bâtiment 505, Campus d'Orsay, 91405 Orsay Cedex, France
[2] Institute of Physics, P.O. Box 304, 10000 Zagreb, Croatia

Received 1st March 2001

Abstract. We propose a new possibility to form ultracold molecules, *via* photoassociation of a pair of cold atoms into vibrational levels of the external well of an excited electronic state located at intermediate interatomic distance (≈ 20 Bohr radii), and embedded in the dissociation continuum above its dissociation limit. The existence of such a well is demonstrated by conventional free-free absorption spectroscopy at thermal energies. Estimation for cold atom photoassociation and cold molecule formation rates are obtained within a perturbative approach [Drag *et al.*, IEEE J. Quant. Electr. **36**, 1378 (2000)], and are found observable for usual conditions of photoassociation experiments.

PACS. 32.80.Pj Optical cooling of atoms; trapping – 34.50.Rk Laser-modified scattering and reactions – 33.80.Ps Optical cooling of molecules; trapping

1 Introduction

In contrast with atoms [1], laser cooling cannot be achieved easily on molecules, as their intrinsic multilevel structure does not allow for a large number of cycles within a closed two-level scheme. Looking for alternative routes to produce molecules with temperatures below $T = E/k_{\rm B} \approx 1$ K ($k_{\rm B}$ is the Boltzmann constant) has become a very active research topic [2] since their first observation no more than three years ago through photoassociation of cold caesium atoms [3], opening up new possibilities to perform unprecedented accurate studies on molecules almost at rest in the laboratory frame (ultrahigh resolution spectroscopy, Bose-Einstein condensation of molecules, molecule laser...). Non-optical procedures are also being investigated, yielding large amounts of molecules but with temperatures ranging between 0.1 to 1 K: the buffer gas cooling technique, and subsequent magnetic trapping has been demonstrated on CaH [4,5]. A beam of neutral dipolar molecules (CO, NH_3) has been also successfully slowed down using a Stark decelerator and trapped in a travelling potential well [6,7].

Up to now, the coolest molecules (with temperature down to $T = E/k_{\rm B} \approx 20$ μK) [3] have been formed through photoassociation (PA) reaction in a cold alkali atom trap, where a pair of cold atoms A in their ground state, separated by a large distance R, absorbs a photon with a frequency slightly red-detuned by $\delta_{\rm red} > 0$ from an atomic transition ν_0, to populate a rovibrational level (v, J) of a long-range excited electronic molecular state Ω with radiative lifetime in the nanosecond range:

$$A + A + h(\nu_0 - \delta_{\rm red}) \rightarrow A_2^*(\Omega; v, J). \qquad (1)$$

Spontaneous emission then occurs mostly at large distances (Fig. 1a), *i.e.* beyond $50a_0$ ($a_0 = 0.0529177$ nm), leaving either a pair of cold atoms with a relative kinetic energy $E_{\rm c} \approx h(\nu_0 - \delta_{\rm red} - \nu_{\rm se})$ large enough to let them escape from the trap:

$$A_2^*(\Omega; v, J) \rightarrow A + A + h\nu_{\rm se}, \qquad (2)$$

or a bound molecule in a rovibrational level (v'', J'') of a lower (long-lived) electronic state α, with an almost unchanged kinetic energy (≈ 0):

$$A_2^*(\Omega; v, J) \rightarrow A_2(\alpha; v'', J'') + h\nu'_{\rm se}. \qquad (3)$$

For alkali dimers the α symbol holds for both the $X^1\Sigma_g^+$ electronic ground state, and the $a^3\Sigma_u^+$ lowest triplet state. In general, process (2) is expected to be the most favoured, while only the few highest vibrational levels very close to the dissociation limit of the X state will have some chance to be populated [8]. Modifying this branching ratio implies to find ways of bringing larger amounts of probability density at shorter internuclear distances (*i.e.* below $20a_0$), increasing the emission probability towards deeper levels of the lowest molecular states. Such possibility has been indeed demonstrated in several experiments using cold traps of caesium [3], and rubidium [9]. The corresponding dimers exhibit in some excited states (labelled by their Hund's case c molecular symmetry 0_g^- and 1_u) secondary shallow potential wells located at internuclear distances where

[a] e-mail: olivier.dulieu@lac.u-psud.fr

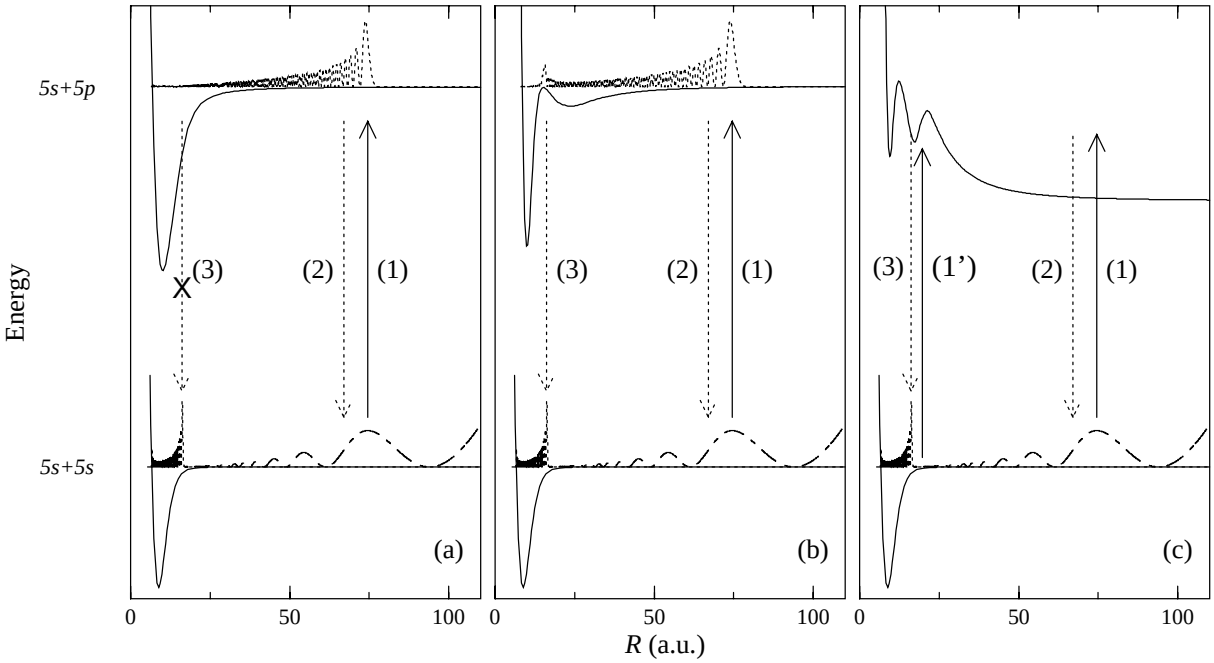

Fig. 1. Photoassociation from the rubidium $5s+5s$ continuum [reaction (1)] to (a) a typical long-range attractive potential; (b) a double-well potential, attractive at long-distance [*e.g.* $0_g^-(5\mathrm{S}+5\mathrm{P}_{3/2})$]; (c) a double-well potential, repulsive at long-distance [*e.g.* $0_g^+(5\mathrm{S}+5\mathrm{P}_{3/2})$]. The system decays by spontaneous emission either back to the continuum [reaction (2)] or to a bound level of a lower electronics state [reaction (3), *e.g.* the $a^3\Sigma_u^+$ state]. For case (a), reaction (3) is usually unlikely.

spontaneous emission toward a wide distribution of bound levels is enhanced, due to the accumulation of probability density around their inner wall in the 15–$25a_0$ range (Fig. 1b). A rate for cold molecule formation as high as a few million molecules per second has been achieved, with a temperature close to the one of the atoms (≈ 100 μK or less). More recently, an efficient new formation mechanism based on resonant coupling between levels of interacting electronic states has been demonstrated [10]. Using two-color excitation of higher electronic states, a similar rate has been also reached for the formation of ultracold K_2 molecule from cold trapped potassium atoms [11]. A multistep procedure has also been investigated theoretically for cold lithium atoms, including a careful quantitative analysis of the populated levels in the molecular ground state [12].

Despite these successful experiments, further developments are still needed, in order to establish other mechanisms for cold molecule formation, either more general, or of different kind, possibly in different species. For instance, all optical procedures implemented up to now used red-detuned lasers for the PA step. In the present work, we address the possibility to form cold molecules using blue-detuned PA laser. Indeed, in a previous theoretical work [13], hereafter referred to as paper I, three of us investigated the properties of "intermediate long-range" potential wells, lying *above* their dissociation limit, and which are predicted in several alkali dimers.

In the K_2 and Rb_2 molecules, such wells are embedded in dissociation continua (Fig. 1c), giving in general a finite lifetime to the bound levels they support. The main difference with the previous situation lies in (i) the smaller extension in internuclear distance of those wells (located typically between 15–$20a_0$), and in (ii) the excitation frequency $\nu_0 + \delta_{\mathrm{blue}}$, $\delta_{\mathrm{blue}} > 0$ which is now blue-detuned from the atomic resonance.

The purpose of the present paper is to establish these systems as potential candidates for photoassociation and ultracold molecule formation experiments. After a brief description of the predicted properties of such "intermediate long-range" wells (Sect. 2), their existence is demonstrated for the first time in Rb_2, through absorption coefficient measurements at thermal energies (Sect. 3). Similar investigations have been previously reported on K_2 [14]. Computation of photoassociation and cold molecule formation rates are then performed (Sect. 4), according to a perturbative approach whose accuracy has been checked on caesium experiments [15]. A discussion on the efficiency of these intermediate long-range potential wells for cold molecule production is then proposed in Section 5.

2 The 0_g^+ intermediate long-range potential wells in alkali dimers

Homonuclear alkali dimers display, among other states converging towards the first excited $ns + np$ dissociation limit, two long-range repulsive states with $^1\Sigma_g^+$ and $^3\Pi_g$ symmetry, varying as C_3/R^3 (with $C_3 > 0$). Due to the ratio $C_3^\Sigma/C_3^\Pi = 2$, and provided that the spin-orbit interaction is strong enough (*i.e.* for all alkalis except Li and Na), these states are expected to mix together to

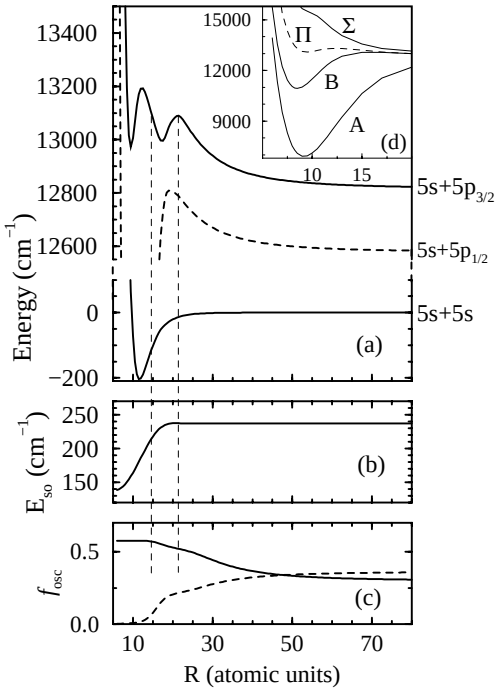

Fig. 2. (a) The $a^3\Sigma_u^+(5S+5S)$ and $0_g^+(5S+5P_{1/2,3/2})$ Rb_2 potentials, used in the present study. (b) The R-variable spin-orbit matrix element included in the diagonalization of the Hamiltonian for the 0_g^+ symmetry, determined by scaling to the Cs_2 case (see text). (c) Oscillator strengths for the $0_g^+(5S+5P_{1/2,3/2}) \rightarrow a^3\Sigma_u^+(5S+5S)$ transitions. Solid lines and broken lines corresponds to states linked to the $(5S+5P_{3/2})$ and $(5S+5P_{1/2})$ limit respectively. (d) Global view of some potentials correlated to the $5s+5p$ limit: $^1\Sigma_g^+$ and $^3\Pi_g$ potentials (denoted by Σ and Π) involved in the 0_g^+ potentials, and $A^1\Sigma_u^+$ and $B^1\Pi_u$ potentials, labelled by A and B respectively.

create a couple of 0_g^+ molecular states, exhibiting an avoiding crossing within the 15–20a_0 range [14,16]. A close-up of the corresponding potentials for the Rb_2 molecule is displayed in Figure 2a. They are identical to those used in paper I. Briefly, they are deduced from the diagonalization, for a given internuclear distance, of the Hamiltonian $H_0 + V_{so}$, where H_0 describes the Hund's case a states $^1\Sigma_g^+$ and $^3\Pi_g$, and V_{so} the spin-orbit coupling operator, taken here as a constant equal to the atomic value $(\sqrt{2}/3)\Delta E_{fs}$ ($\Delta E_{fs} = 237.6$ cm^{-1} for Rb). Hund's case a curves are built from quantum chemistry calculations [17], matched with long-range asymptotic calculations [18]. A shallow outer potential well is now present in the upper $0_g^+(P_{3/2})$ potential curve, dissociating into $Rb(5S)+Rb(5P_{3/2})$. According to paper I, it is located around $17a_0$, and due to the repulsive character of the molecular states, it is fully embedded in the dissociation continuum of both dissociation limits $5S+5P_{1/2,3/2}$. A well depth $D_e \approx 93$ cm^{-1} is predicted, allowing the existence of 11 bound levels, the two uppermost ones undergoing dissociation *via* tunnel effect towards large distances. We predicted also a similar pattern in K_2, but the potential well is shallower ($D_e \approx 42$ cm^{-1}), and supports only 2 or 3 quasibound levels, strongly dissociating *via* both tunneling through the $0_g^+(P_{3/2})$ barrier, and predissociation into the $0_g^+(P_{1/2})$ state. In contrast, only a shoulder is expected in the $0_g^+(P_{3/2})$ potential in Cs_2.

The spectroscopy of these levels has never been achieved. However, it is now possible to detect their existence in Rb_2 through free-free absorption experiments at thermal energies, as reported in the next section. Similar studies have also been performed on K_2 [14] and more recently for Cs_2 [19]. Furthermore, starting from a pair of cold atoms, the efficiency of the cold molecule formation in levels of the $a^3\Sigma_u^+(5s+5s)$ state will result from the cooperation of the (free-bound) photoassociation, mostly favoured at large distances, and the spontaneous emission toward bound levels of the triplet state, which will occur within the (15–20a_0) range (see for example Ref. [20]).

For the present calculations, we chose the variable molecular spin-orbit coupling drawn in Figure 2b. Due to the lack of available quantum chemistry calculation for this quantity for Rb_2, we obtained it by scaling to the Cs_2 case taken from reference [21]. Its magnitude displays a marked R-dependence going from the asymptotic region toward the equilibrium distance, but remains almost constant over the region of the $0_g^+(P_{3/2})$ external well, only changing slightly the potential curves of Figure 2a (not visible on the figure scale). The oscillator strength for the transition between the excited $0_g^+(P_{3/2})$ state and the lowest $a^3\Sigma_u^+(5s+5s)$ state, computed from asymptotic model [22] is drawn in Figure 2c. It increases as the state comes close to the excited $^3\Pi_g(5s+5p)$ state. Conversely, the transition moment involving the $0_g^+(P_{1/2})$ state is vanishing as the $^1\Sigma_g^+(5s+5p)$ character becomes dominant with decreasing distances.

The excitation of the bound levels of the $0_g^+(P_{3/2})$ state from a pair of colliding ground state atoms will then be strongly influenced by the two following issues: first, the external well is quite narrow, which will restrict the radiative transitions involving the bound levels within a limited range (15–20a_0) of internuclear distances. Second, the branching ratio between free-bound and free-free absorption, strongly depends on the relative velocity of the atoms. Therefore it is worthwhile to investigate the spectroscopy of this intermediate long-range state to improve the knowledge of the related molecular data. We present in the following section experimental results obtained through free-free absorption spectroscopy at thermal energies, while we propose in Section 4 an experiment based on photoassociation spectroscopy of cold Rb atoms with blue detuned laser light, showing that ultracold molecule formation can be expected.

3 The $0_g^+(P_{3/2})$ state probed by free-free absorption at thermal energies

Absorption spectra of diatomic molecules have been shown for a long time to be governed by the behaviour of the so-called Mulliken's potentials, or difference potentials [23], and have been extensively reviewed by Tellinghuisen [24].

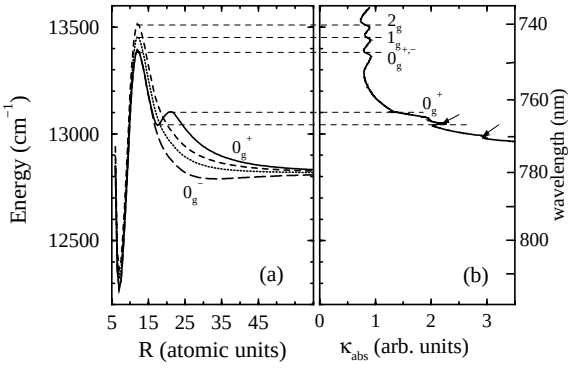

Fig. 3. (a) Difference potentials for the $^3\Pi_g(0_g^+, 0_g^-, 1_g, 2_g) \rightarrow a^3\Sigma_u^+(5S+5S)$ transitions. (b) Experimental absorption coefficient at 650 K, the density being 1.1×10^{17} cm^{-3}. Dashed lines indicate the correspondence between extrema in a given symmetry with structures observed in the spectrum. Arrows show features assigned to the presence of potassium impurities. The wavelength scale is also displayed on the left.

Such an analysis is based on the Franck-Condon principle. The existence of one or several extrema in the difference between the two electronic potentials involved in a given absorption transition induces, at a given energy, the presence of several Condon points, contributing to the absorption probability through interference patterns. They are responsible for the "satellite bands", or pronounced shoulders in the wings of the self-broadened spectral lines. Difference potentials corresponding to the dipole transition $a^3\Sigma_u^+ \rightarrow 0_g^+(P_{3/2})$ in Rb_2 are reproduced in Figure 3a, deduced from data displayed in Figure 2. Four extrema are found, located around $7a_0$, $12a_0$, $17a_0$ and $21a_0$, respectively. Their influence in the absorption spectrum will be discussed below. Let us notice that the double minimum potential will give rise to the contribution of three or four interfering Condon points in the 765 nm region.

Two of the authors of the present paper have long been working on performing absorption experiments in alkali vapors at thermal energies. Their group has been successful in determining the position of many diffuse bands in alkali dimers (see Ref. [25] and references therein, and [19]). Semiclassical computations of the corresponding absorption coefficients have also been proposed, showing that the results are very sensitive to the choice of the difference potentials included in the model. The accuracy of the measurements allow to fit these potentials at a few cm^{-1} scale, which is remarkable for free-free spectroscopy at thermal energies. The satellite band for the transition $a^3\Sigma_u^+ \rightarrow 0_g^+(P_{3/2})$ in K_2 has also been observed many years ago [26], and more recently in Cs_2 [19]. It should be noted that existing theoretical calculations [21] show that $0_g^+(P_{3/2})$ potential in Cs_2 is not exhibiting a double minimum shape, whereas the corresponding $0_g^+(P_{3/2}) - a^3\Sigma_u^+$ difference potential is indeed a double minimum curve. The complete experimental and theoretical work concerning both $0_g^+(P_{3/2}) - a^3\Sigma_u^+$ and $0_g^+(P_{1/2}) - a^3\Sigma_u^+$ transitions will be discussed in detail in a forthcoming publication [27]. In the following, we report on the observation of this transition in Rb_2, probing for the first time the presence of the double well structure of the $0_g^+(P_{3/2})$ state in Rb_2, then making worth its study through photoassociation spectroscopy.

We performed a simple absorption experiment with dense rubidium vapor generated in a heat-pipe oven at several temperatures, up to 650 K (at a density of 1.1×10^{17} cm^{-3}). A scheme of this experiment can be found in reference [25]. We used a tungsten-halogen lamp as a background light source of white light, which was spectrally analyzed by a high resolution scanning monochromator after passing through a heat-pipe oven. The portion of the absorption spectrum in the quasistatic blue wing of the self-broadened rubidium resonance line at 780 nm is shown in Figure 3b for a temperature of 650 K. The strongest structures are observed at 650 K, with three distinct peaks located at about 739.8, 744.1 and 748.1 nm. They were first observed by Awan and Lewis [28] and later interpreted as stemming from the $a^3\Sigma_u^+ \rightarrow (1)^3\Pi_g$ transition [26]. The difference potential curves in Figure 3a, reported on the same scale, exhibit the triplet structure of the $(1)^3\Pi_g$ state, which splits into 2_g, 1_g and close lying 0_g^- and 0_g^+ states due to spin-orbit interaction. The corresponding three distinct maxima around $12a_0$ in the $2_g - a^3\Sigma_u^+$, $1_g - a^3\Sigma_u^+$, and $0_g^{+/-} - a^3\Sigma_u^+$ difference potential curves are responsible for the enhancement of the absorption coefficient at 739.8, 744.1 and 748.1 nm, in the blue wing of the 780 nm line. Another interesting and peculiar satellite band with two shoulders at 764 and 765 nm is also found, located right in front of the double well structure of the $0_g^+(P_{3/2}) - a^3\Sigma_u^+$ difference potential induced by the $0_g^+(P_{3/2})$ external well (see horizontal dashed lines in Fig. 3). A similar interpretation has already been given for the analogous case in K_2 [14,26]. Let us mention that the small peaks located in the same zone (marked with arrows in Fig. 3) are due to almost unavoidable potassium traces in the heat-pipe oven.

In order to check more precisely this hypothesis, and the relevant difference potential curves, we have computed the reduced absorption coefficient $\kappa'_{abs}(\lambda, T)$ (*i.e.* the absorption rate per unit of photon flux and per unit density, expressed in cm^5) in the range of wavelength λ of the quasistatic blue wing of rubidium 780 nm line, at $T = 650$ K. We used the same quasiclassical approach outlined in the recent study of caesium satellite bands associated to the $a^3\Sigma_u^+ \rightarrow (3)^3\Pi_g(0_g^{+,-}, 1_g, 2_g)$ transition [29], also involving double well feature in the difference potentials.

The computed reduced absorption coefficient $\kappa_{abs}(\lambda, T)$ consists in added contributions of singlet and triplet excited states correlated to the $5s + 5p$ dissociation limit. Results are reproduced in Figure 4, together with the experimental coefficient $\kappa'_{exp}(\lambda, T)$ at 650 K. The global uncertainty on the absolute value is of about 20%, while the relative precision does not exceed the thickness of the line. The singlet contribution (line (i) in Fig. 4) includes the absorption into the $A^1\Sigma_u^+$, $B^1\Pi_u$, and $(2)^3\Sigma_u^+(1_u)$ states, starting from the $X^1\Sigma_g^+$ ground state. The corresponding excited states are recalled to guide the eye in the inset of Figure 2, labelled by A, B

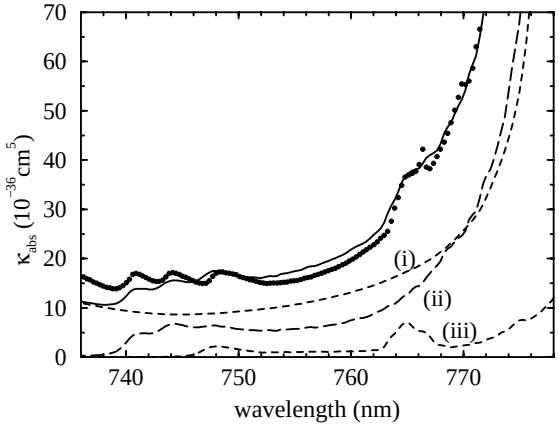

Fig. 4. Absorption coefficients at $T = 650$ K. Closed circles: experimental; Solid line: computed. The other lines correspond to calculations including (i) excited singlet state contribution only , (ii) $^3\Pi_g(0_g^-, 1_g, 2_g)$ states contribution only, (iii) $^3\Pi_g(0_g^+$ state contribution only.

and Σ respectively. There is an increasing importance of B–X band toward smaller wavelengths, and an increasing importance of A–X band toward longer wavelengths, whereas $(2)^3\Sigma_u^+(1_u)$–X band contributes only close to the Rb 780 nm line center (*i.e.* at large internuclear distances), due to the rapid fall off of the corresponding transition dipole moment toward the blue spectral region as it becomes a forbidden transition. The triplet contribution (line (ii) in Fig. 4) involves the transitions toward the excited $(1)^3\Pi_g(0_g^-, 1_g, 2_g)$ manifold (labelled by Π in the inset of Fig. 2) starting from the lowest $a^3\Sigma_u^+$ state. We see that the three maxima in the 740–750 nm range are well reproduced. This is mainly a consequence of the fact that we introduced in our diagonalization procedure a spin-orbit interaction that depends on internuclear separation. The curve labelled (iii) in the same figure represents the individual contribution of the $0_g^+(\mathrm{P}_{3/2}) - a^3\Sigma_u^+$ transition, characterized by the double minimum difference potential. The satellite band at 748.1 nm (*i.e.* the third maxima quoted above in curve (ii)) lies at the same wavelength as the one for the $0_g^-(\mathrm{P}_{3/2}) - a^3\Sigma_u^+$, whereas the two partly merged satellite bands at 764 and 765 nm are also clearly seen. Experimental and theoretically calculated rate coefficients compare very well considering the nature of our quasiclassical calculations in which we used *ab initio* potential curves, transition dipole moment functions and variable spin-orbit interaction.

4 Computation of photoassociation and cold molecule formation rates

As demonstrated in paper I, the $0_g^+(\mathrm{P}_{3/2})$ state in Rb_2 can be considered independently from its $0_g^+(\mathrm{P}_{1/2})$ partner, as beside spontaneous emission, only decay of the vibrational levels of the external well by tunneling through the barrier towards large distances is expected. The photoassociation of cold Rb atoms from the continuum of the lowest triplet state $a^3\Sigma_u^+$, denoted as a for brievety, into levels of the $0_g^+(\mathrm{P}_{3/2})$ external well (hyperfine structure is neglected here), requires blue-detuned laser light, *i.e.* with frequency $\nu_{\mathrm{blue}} = \nu_0 + \delta_{\mathrm{blue}}$, with $\delta_{\mathrm{blue}} > 0$. Then for a given level v, the absorption coefficient (expressed in cm^{-1}) writes formally:

$$\kappa_{\mathrm{abs}}(\delta_{\mathrm{blue}}) = \kappa_{\mathrm{PA}}(\delta_{\mathrm{blue}}) + \kappa_{\mathrm{abs}}^{\mathrm{ff}}(\delta_{\mathrm{blue}}) \qquad (4)$$

where κ_{PA} is the (free-bound) PA coefficient, and $\kappa_{\mathrm{abs}}^{\mathrm{ff}}$ the competing free-free absorption coefficient into the $5\mathrm{S} + 5\mathrm{P}_{3/2}$ dissociation continuum, at the same detuning δ_{blue}. In a quantum approach, these coefficients are depending upon the overlap between radial wavefunction of the initial collisional state, and the wavefunction of the final bound level or of the final dissociating state, respectively. We have seen in Section 3 that due to the large width of the thermal energy distribution, the free-free contribution dominates the absorption process. The context of cold atom collisions is now very different. The initial relative kinetic energy distribution of cold atoms is so sharp ($E/h \approx 5$ MHz, or $E/k_{\mathrm{B}} = T \approx 0.1$ mK) that the initial collisional state can safely be considered as a quasi-discrete state, yielding to the photoassociation transition an almost resonant character. This feature represents the basis of the efficiency of cold atom photoassociation as a powerful tool for molecular spectroscopy (see for example [30]). Similarly, a single free-free absorption can be considered as a transition between two quasidiscrete levels. Describing the balance between photoassociation into a level v_{e} of the $0_g^+(\mathrm{P}_{3/2})$ outer well (with vibrational wavefunction $\chi(v;R)$) and the related dissociation continuum (with wavefunction $(\phi_{\mathrm{e}}(E'))$ will then require the computation of (i) the free-bound matrix elements $\langle\phi_{\mathrm{a}}(E)|D_{\mathrm{ae}}(R)|v_{\mathrm{e}}\rangle$, where $\phi_{\mathrm{a}}(E;R)$ is the continuum radial wavefunction for the initial pair of atoms with energy $E = k_{\mathrm{B}}T$, and $D_{\mathrm{ae}}(R)$ the electronic transition dipole moment, (ii) the free-free matrix element $\langle\phi_{\mathrm{a}}(E)|D_{\mathrm{ae}}(R)|\phi_{\mathrm{e}}(E')\rangle$, taken for the single energy $E' \equiv E_v$, relative to the $5\mathrm{S} + 5\mathrm{P}_{3/2}$ limit.

Assuming that the free-free transition will take place mainly at the turning points of the repulsive curves, the calculation of free-free matrix elements necessitates their evaluation for a distribution of energies of the dissociation continuum of all states $0_g^{+,-}, 1_g, 2_g(\mathrm{P}_{3/2})$ around each bound level of the $0_g^+(\mathrm{P}_{3/2})$ outer well. As in the ground state, this distribution could be approximated by a single stationary wave at each vibrational energy. As the $0_g^+(\mathrm{P}_{3/2})$ potential curve is almost symmetric around the top of the barrier at $\approx 21a_0$, the magnitude of the free-free matrix element is estimated to be of the same magnitude as the corresponding free-bound matrix element at the same energy [32]. Therefore we assume in the following that rates including only the free-bound transitions are upper limits of the actual rates, which are then overestimated by a factor of about 2 or 3. This hypothesis is actually confirmed by preliminary calculations which will be presented elsewhere [33].

Following recent work in our group [20,31], we calculate below the PA rate $\mathcal{R}_{\mathrm{PA}}$ per atom (expressed in

s^{-1}), related to the absorption coefficient $\kappa_{\rm PA}$ (expressed in cm^{-1}) by:

$$\mathcal{R}_{\rm PA} = \kappa_{\rm PA} \frac{I}{h\nu_{\rm blue}} \quad (5)$$

where I is the intensity of the PA laser with frequency $\nu_{\rm blue}$, all expressed in S.I. units. Let us note that other authors (see for example Ref. [34]) use the reduced absorption coefficient $\kappa'_{\rm PA}$ (expressed in cm^5), similar to the $\kappa'_{\rm abs}$ in Section 3, according to:

$$\mathcal{R}_{\rm PA} = \kappa'_{\rm PA} n_{\rm at}^2 \frac{I}{h\nu_{\rm blue}} \quad (6)$$

where $n_{\rm at}$ is the atomic density of the atomic sample. The PA rate $\mathcal{R}_{\rm PA}$ is evaluated according to the perturbative approach of reference [31], and recently checked against experimental measurements [20]:

$$\mathcal{R}_{\rm PA}(\delta_{\rm blue}) = \left(\frac{3}{2\pi}\right)^{\frac{3}{2}} \frac{h}{2} n_{\rm at} \lambda_{\rm th}^3 K^2 \mathcal{A} \left|\langle v(0_g^+)|\zeta(R)|\phi_{\rm a}(E)\rangle\right|^2, \quad (7)$$

where $\lambda_{\rm th} = h\sqrt{1/(3\mu kT)}$ is the thermal de Broglie wavelength (μ is the reduced mass of the system), $2K = 2K_0\sqrt{I/I_0}$ the atomic Rabi frequency for an intensity of I, $2K_0 = \Gamma/\sqrt{2}$ the Rabi frequency at saturation intensity I_0, Γ the atomic excited state linewidth and $\mathcal{A}$ an angular factor accounting for hyperfine degeneracy and orientation averaging. The function $\zeta(R)$, normalized to 1 at large distances, accounts for the variation of the transition dipole moment according to Figure 2c. The rate of formation of cold molecules $\mathcal{R}_{\rm mol}$ is then obtained by considering the total probability that the photoassociated atom pair decays (by spontaneous emission) towards all bound levels $|v'(a)\rangle$ of the $a^3\Sigma_u^+$ electronic state, *i.e.*,

$$\mathcal{R}_{\rm mol}(\delta_{\rm blue}) = \mathcal{R}_{\rm PA}(\delta_{\rm blue}) \sum_{v'} \left|\langle v(0_g^+)|\zeta(R)|v'(a)\rangle\right|^2, \quad (8)$$

where the sum runs over all vibrational levels v' of the $a^3\Sigma_u^+$ state, again including the R-dependence of the transition dipole moment through the ζ function. In equations (7, 8), the $a^3\Sigma_u^+$ potential is taken from reference [17], connected at long range to a C_n/R^n expansion including $n = 6, 8, 10$ terms. We chose the most recent determination for $C_6 = -4\,700$ a.u. [35], and the C_8, C_{10} values from reference [18]. The repulsive wall of the $a^3\Sigma_u^+$ potential curve has been adjusted to yield scattering lengths values $a_{\rm T} = -370a_0$ for $^{85}Rb_2$ and $a_{\rm T} = 109a_0$ for $^{87}Rb_2$ respectively, in accordance with reported experimental determinations $a_{\rm T}(^{85}{\rm Rb}) = -369 \pm 16a_0$ and $a_{\rm T}(^{87}{\rm Rb}) = 106 \pm 4a_0$ [35].

Computed rates $\mathcal{R}_{\rm PA}/\mathcal{A}$ and $\mathcal{R}_{\rm mol}/\mathcal{A}$ are displayed in Figure 5 for both cases $\zeta = 1$ or variable $\zeta(R)$, reflecting the magnitude of the R-dependence of the transition moment (Fig. 2c). Parameters for typical experimental conditions [9] are introduced, *i.e.* $T = 120$ μK, $n_{\rm at} = 3 \times 10^{10}$ cm^{-3}, and $I = 10$ $W\,cm^{-2}$. Only the s-wave contribution is considered. Other parameters are $I_0 = 1.5$ $mW\,cm^{-2}$ and $\Gamma = 5.9$ MHz. The PA rates exhibit minima and maxima, related to the position of the nodes in the initial continuum s-wavefunction [34,36]. As already observed in recent work [37], maxima of the $^{85}Rb_2$ rates roughly corresponds to minima in the $^{87}Rb_2$ rates, due to different scattering length of the lowest triplet state. The sum of overlap factors between a 0_g^+ vibrational level v and the $a^3\Sigma_u^+$ vibrational levels, present in equation (8), and displayed in Figure 5b:

$$\mathcal{S}(v) = \sum_{v'} \left|\langle v(0_g^+)|\zeta|v'(a)\rangle\right|^2 \quad (9)$$

are slowly varying between ≈ 0.3 up to 1, and confirm that 0_g^+ levels are indeed good candidates for cold molecule formation with blue detuned laser light. Resulting cold molecule rates are also reported in Figure 5b, showing a variation similar to $\mathcal{R}_{\rm PA}$. It is striking to see that maxima in $\mathcal{R}_{\rm mol}$ or in $\mathcal{R}_{\rm PA}$ for the ^{85}Rb isotope are roughly

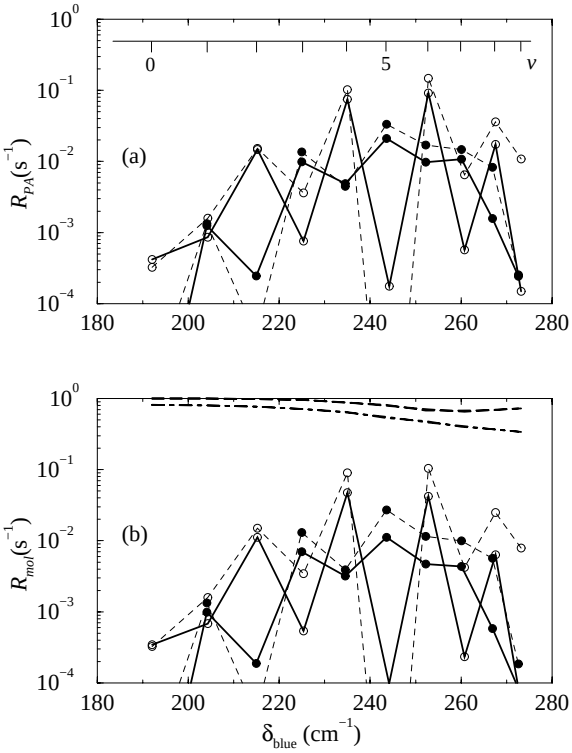

Fig. 5. (a) Photoassociation rate per atom $\mathcal{R}_{\rm PA}$ and (b) cold molecule formation rate per atom $\mathcal{R}_{\rm mol}$, as a function of the detuning $\delta_{\rm blue}$ of the PA laser, for the external well of the $0_g^+(P_{3/2})$ state. 0_g^+ levels up to $v = 9$ are considered. Typical experimental conditions of a Rb magneto-optical trap are assumed, *i.e.* $I = 10$ W/cm^2, $n_{\rm at} = 3 \times 10^{10}$ cm^{-3}, $T = 120$ μK. Both isotopes ^{85}Rb (open circles) and ^{87}Rb (closed circles) are considered. Calculations without (dashed lines) and with (solid lines) inclusion of a variable transition dipole moment are displayed. In panel (b) the sum of Franck-Condon factors involved in equations (8, 9), without (long dashed line) and with (dot-dashed line) inclusion of a variable transition dipole moment, are shown on the same scale.

4 to 5 times larger than for the ^{87}Rb isotope, as already predicted for the $0_g^-(P_{3/2})$ long-range state [37]. This is mainly due to the the different amplitude of the continuum wavefunction at such internuclear distances, induced by difference between the scattering length of the two isotopes.

On a more quantitative basis, the formation of ultracold molecule *via* photoassociation of the $0_g^-(P_{3/2})$ long-range state in caesium [20] or rubidium [37], can be used as benchmarks for estimation of the efficiency of the present situation. Assuming for rubidium a value $\mathcal{A} \approx 0.01$ similar to the caesium one [20], and considering the typical experimental conditions quoted above, the obtained formation rates are $\mathcal{R}_{\rm mol}^{\rm Cs}(0_g^-) \sim 0.007$ s^{-1} [20] and $\mathcal{R}_{\rm mol}^{^{87}{\rm Rb}}(0_g^-) \sim 0.001$–$0.005$ s^{-1} [37]. Under the same assumptions, the maximum values obtained here for the 0_g^+ state are 0.0001 s^{-1} and 0.0004 s^{-1}. Despite this apparently unfavourable ratio compared to the 0_g^- channel, the formation of ultracold molecules *via* PA of the $0_g^+(P_{3/2})$ state is worthwhile to try. Indeed, it is currently possible to optimize experimental conditions comparable to the caesium case: the density could then be increased by a factor of ≈ 3, and the intensity by a factor of ≈ 10, for which the PA transition saturates in caesium [3]. In the present case, as the free-free absorption contributes as a loss channel, the saturation would be reached at even larger intensities. Then a cold molecule rate close to or larger than the one observed for the $0_g^-(P_{3/2})$ state in Rb_2 could be expected. Furthermore, the distribution of $a^3\Sigma_u^+$ vibrational levels populated after spontaneous emission from 0_g^+ and 0_g^- external well levels will strongly differ, as the 0_g^+ well lies at shorter distances than the 0_g^- well. Fioretti *et al.* [37] demonstrated that only the uppermost $a^3\Sigma_u^+$ levels (bound by about 1 cm^{-1}) are populated after spontaneous decay of the $0_g^-(P_{3/2})$ rubidium state. In contrast, the present computations, displayed in Figure 6 for a few photoassociated levels lying in the $0_g^+(P_{3/2})$ external well, show that much deeper levels (with binding energies up to ≈ 80 cm^{-1}) are populated in the lowest triplet state. The vibrational distribution of the ultracold molecules is then expected to peak at quite small vibrational quantum number, say down to $v \approx 15$.

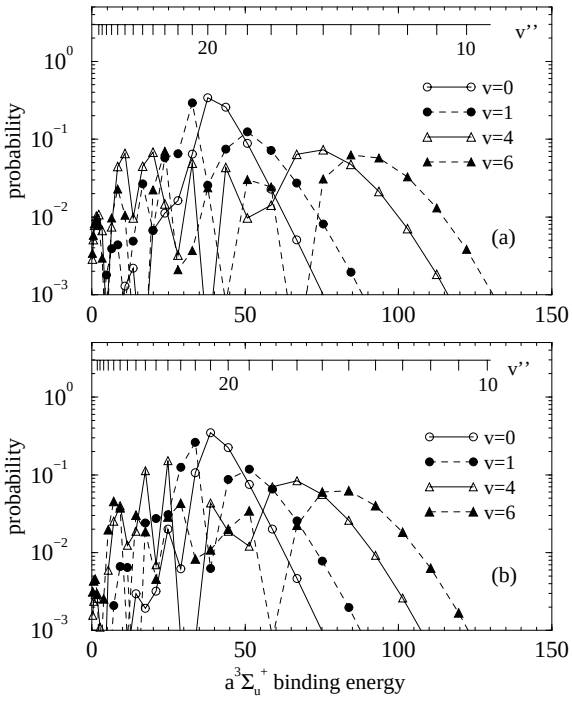

Fig. 6. Computed distributions on the vibrational levels v'' in the lowest triplet state of (a) $^{85}Rb_2$, (b) $^{87}Rb_2$ cold molecules, for selected $0_g^+(P_{3/2})$ vibrational levels v.

5 Discussion and conclusion

Beside ultracold molecule formation, photoassociation into levels of the $0_g^+(P_{3/2})$ outer well would provide an intermediate "Franck-Condon window" for absorption towards higher Rb_2 electronic states [38]. The main question is, of course, whether a sufficiently large number of ultra-cold Rb atomic pairs can be found at the distance of about $20a_0$, where the absorption into the outer well of the $0_g^+(P_{3/2})$ state occurs. Only s-wave collisions are included in the above calculations, and the centrifugal barrier acting during p- or d-wave collisions will prevent atoms to come close enough to undergo an absorption into levels of this well. Therefore for such experiments to be feasible it would be necessary to have extremely low temperatures, where the s-wave is predominant.

Our calculations show also that the Rb atom density should be as high as possible. Several possibilities for enhancing the density of ultracold rubidium atoms can be considered, based on very recent experimental developments. Friedman *et al.* [39] demonstrated a compression of cold atoms to very high densities in a rotating-beam blue-detuned optical trap. The trap loaded with more than 10^6 Rb atoms was compressed adiabatically by a factor of 350 to a final density of 5×10^{13} cm^{-3}. The two-body elastic and inelastic collision rates of atoms in the compressed trap play an important role and the atomic cloud becomes one-dimensional. However, this kind of a trap is promising for applications to trapping of ultra-cold molecules as well [40]. In the near future rotating blue detuned laser could be one of the technique capable to compress initial ultracold cloud to densities up to 10^{14} cm^{-3} [39]. The main trick of the method would be to decrease the radius of the rotating laser to a most appropriate value at which there is still not appreciable push of the cloud. If the blue-detuned laser beam is vertical and point upwards at the final radius it is possible to shine the additional 765 nm laser in order to excite the outer well of the Rb_2 $0_g^+(P_{3/2})$ state. The nascent Rb_2 $0_g^+(P_{3/2})$ molecules will remain at the position of the original cloud, and will be confined by the dynamical blue detuned optical trap. It is possible that these molecules will be also formed during the upward motion of ultracold rubidium atoms, thus making rubidium molecular fountain possible.

Another possibility is connected with Bose-Einstein condensate as a starting point of the ultracold cloud with large rubidium atom densities. Recently, Wynar *et al.* [41] created state selected $^{87}Rb_2$ molecules almost at rest in a Bose-Einstein condensate of rubidium atoms. They used coherent free-bound-bound stimulated Raman pumping technique at densities of up to about 3×10^{14} cm^{-3}. We believe that a similar method could be applied even for the blue-detuned free-bound-bound Raman pumping in order to create triplet ground state Rb_2 molecules by using the first laser transition to excite the bound states in the outer well of the Rb_2 $0_g^+(P_{3/2})$ molecules.

We should mention another way of detecting cold Rb_2 $0_g^+(P_{3/2})$ molecules. In experiments with superfluid He clusters going through alkali pick-up cells, Scoles and coworkers [42] have observed Li_2, Na_2 and K_2 molecules in their lowest triplet states. It is quite possible that in an analogous experiment, where rubidium is put in the pick-up cell, the Rb_2 $0_g^+(P_{3/2})$ bound states in the outer potential well can be easily excited. It would be interesting to study such transitions when a Rb_2 triplet molecule is attached to the cold helium cluster, or when it freely copropagates detached from the parent cluster. Ernst [43] recently succeeded to observe low resolution triplet spectrum from Rb_2 molecules attached at the surface of the superfluid helium droplets. Although his observations were at shorter wavelengths than in the present work, the findings clearly show the way for the observation of Rb_2 $0_g^+(P_{3/2})$ state attached on a helium nanocryostat in a near future.

In conclusion we have identified an intermediate long-range Rb_2 molecule, which could be excited by photoassociation of cold Rb atoms, using photons detuned to the blue of the resonant D_2 atomic transition. Excited levels would be those lying in the outer well of the $0_g^+(P_{3/2})$ double minimum potential, embedded entirely within the $5S + 5P_{3/2}$ dissociation continuum. The existence of this intermediate long-range Rb_2 molecule is probed experimentally for the first time, using free-free absorption at thermal energies. This result is also confirmed by quasi-classical simulations of the absorption coefficient. Such a well may be efficiently used as an intermediate state opening a narrow Frank-Condon window that enables further excitation to higher state at distances of about $20a_0$. Furthermore, the PA rate into this outer well in ultracold conditions is fair, and the probability of the formation of stable ultracold rubidium molecules in their lowest triplet state is encouraging, especially if higher atom densities could be achieved for the cold atomic cloud. The formed ultracold molecules are predicted to be stabilized in vibrational levels much deeper than those populated in the experiment by Gabbanini *et al.* [9] relying on PA into the long-range $0_g^-(P_{3/2})$ state of Rb_2. A two-color PA experiment could be realized, combining PA into the $0_g^-(P_{3/2})$ state, followed by spontaneous emission, with excitation of the formed cold molecules into the outer well of the $0_g^+(P_{3/2})$ state, producing itself ultracold molecules. The whole process will recycle the vibrational distribution of the ultracold molecules toward low vibrational levels, with binding energies up to ≈ 80 cm^{-1}.

Claude Amiot and Claude Dion are gratefully acknowledged for stimulating discussions. G.P. acknowledges Laboratoire Aimé Cotton and CNRS for a three-month invitation. The work in Zagreb was supported by Ministry of Sciences and Technology of Republic of Croatia.

References

1. H. Metcalf, P. van der Straten, Phys. Rep. **244**, 203 (1994).
2. J.T. Bahns, P.L. Gould, W.C. Stwalley, Adv. At. Mol. Phys. **42**, 71 (2000).
3. A. Fioretti, D. Comparat, A. Crubellier, O. Dulieu, F. Masnou-Seeuws, P. Pillet, Phys. Rev. Lett. **80**, 4402 (1998).
4. J.D. Weinstein, R. deCarvalho, T. Guillet, B. Friedrich, J.M. Doyle, Nature **395**, 148 (1998).
5. R. deCarvalho, J.M. Doyle, B. Friedrich, T. Guillet, J. Kim, D. Patterson, J.D. Weinstein, Eur. Phys. J. D **7**, 289 (1999).
6. H.L. Bethlem, G. Berden, G. Meijer, Phys. Rev. Lett. **83**, 1558 (1999).
7. H.L. Bethlem, G. Berden, A.J.A. van Roij, F.M.H. Crompvoets, G. Meijer, Phys. Rev. Lett. **84**, 5744 (2000).
8. H.R. Thorsheim, J. Weiner, P.S. Julienne, Phys. Rev. Lett. **58**, 2420 (1987).
9. C. Gabbanini, A. Fioretti, A. Lucchesini, S. Gozzini, M. Mazzoni, Phys. Rev. Lett. **84**, 2814 (2000).
10. C.M. Dion, C. Drag, O. Dulieu, B. Laburthe Tolra, F. Masnou-Seeuws, P. Pillet, Phys. Rev. Lett. **86**, 2253 (2001).
11. A.N. Nikolov, J.R. Enscher, E.E. Eyler, H. Wang, W.C. Stwalley, P.L. Gould, Phys. Rev. Lett. **84**, 246 (2000).
12. R. Côté, A. Dalgarno, Chem. Phys. Lett. **279**, 50 (1997).
13. O. Dulieu, R. Kosloff, F. Masnou-Seeuws, G. Pichler, J. Chem. Phys. **107**, 10633 (1997).
14. S. Milošević, R. Beuc, M. Movre, G. Pichler, D. Veža, Fizika (YU), **14**, 345 (1982).
15. C. Drag, B. Laburthe Tolra, O. Dulieu, D. Comparat, M. Vatasescu, S. Boussen, S. Guibal, A. Crubellier, P. Pillet, IEEE J. Quant. Electron. **36**, 1378 (2000).
16. E.I. Dashevskaya, A.I. Voronin, E.E. Nikitin, Can. J. Phys. **47**, 1237 (1969).
17. M. Foucrault, Ph. Millié, J.P. Daudey, J. Chem. Phys. **96**, 1257 (1992).
18. M. Marinescu, A. Dalgarno, Phys. Rev. A **52**, 311 (1995).
19. D. Veža, R. Beuc, S. Milošević, G. Pichler, Eur. Phys. J. D **2**, 45 (1998).
20. C. Drag, B. Laburthe Tolra, O. Dulieu, D. Comparat, M. Vatasescu, S. Boussen, S. Guibal, A. Crubellier, P. Pillet, IEEE J. Quant. Electron. **36**, 1378 (2000).
21. N. Spiess, Ph.D. thesis, Fachbereich Chemie, Universität Kaiserslautern, 1989.
22. M. Vatasescu, Ph.D. thesis, Université Paris-Sud, 1999.
23. R.S. Mulliken, J. Chem. Phys. **55**, 339 (1971).
24. J. Tellinghuisen, *Photodissociation and Photoionization*, edited by K.P. Lawley (John Wiley and Sons Ltd., 1985), p. 229.
25. G. Pichler, S. Milošević, D. Veža, R. Beuc, J. Phys. B: At. Mol. Opt. Phys. **16**, 4619 (1983).
26. R. Beuc, Msc thesis, University of Zagreb, Croatia, 1986.
27. R. Beuc, H. Skenderović, T. Ban, D. Veža, G. Pichler, W. Meyer, Eur. Phys. J. D **15**, 209 (2001).

28. M.S. Awan, E.L. Lewis, J. Phys. B: At. Mol. Opt. Phys. **9**, L551 (1976).
29. T. Ban, H. Skenderović, R. Beuc, G. Pichler, Europhys. Lett. **48**, 378 (1999).
30. W.C. Stwalley, H. Wang, J. Molec. Spect. **195**, 194 (1999).
31. P. Pillet, A. Crubellier, A. Bleton, O. Dulieu, P. Nosbaum, I. Mourachko, F. Masnou-Seeuws, J. Phys. B: At. Mol. Opt. Phys. **30**, 2801 (1997).
32. R. Beuc, unpublished
33. T. Ban, Ph.D. thesis, Zagreb, in progress.
34. R. Côté, A. Dalgarno, Phys. Rev. A **58**, 498 (1998).
35. J.L. Roberts, N.R. Claussen, J.P. Burke, C.H. Greene, E.A. Cornell, C.E. Wieman, Phys. Rev. Lett. **81**, 5109 (1998).
36. C. Drag, B. Laburthe Tolra, B. T'Jampens, D. Comparat, M. Allegrini, A. Crubellier, P. Pillet, Phys. Rev. Lett. **85**, 1408 (2000).
37. A. Fioretti, C. Amiot, C.M. Dion, O. Dulieu, M. Mazzoni, G. Smirne, C. Gabbanini, Eur. Phys. J. D **15**, 189 (2001).
38. H. Wang, X.T. Wang, P.L. Gould, W.C. Stwalley, Phys. Rev. Lett. **78**, 4173 (1997).
39. N. Friedman, L. Khaykovich, R. Ozeri, N. Davidson, Phys. Rev. A **61**, 031403(R) (1998).
40. P. Rudy, R. Ejnisman, A. Raman, S. Lee, N.P. Bigelow, Opt. Expr. **8**, 159 (2001).
41. R. Wynar, R.S. Freeland, D.J. Han, C. Ryu, D.J. Heinzen Science **287**, 1016 (2000).
42. J. Higgins, C. Callegari, J. Reho, F. Stienkemeier, W.E. Ernst, M. Gutowski, G. Scoles J. Phys. Chem. A **102**, 4952 (1998).
43. W. Ernst, private communication.